ELSEVIER

Journal of Nuclear Materials 313–316 (2003) 1123–1130

journal of nuclear materials

www.elsevier.com/locate/jnucmat

Section 8. Divertor, impurity transport and plasma edge control

Control of divertor heat load by Ar injection with keeping high performance in ELMy H-mode plasmas on JT-60U

S. Higashijima *, N. Asakura, H. Kubo, Y. Miura, T. Nakano, S. Konoshima, K. Itami, S. Sakurai, H. Takenaga, H. Tamai, The JT-60 Team

Japan Atomic Energy Research Institute, Naka Fusion Research Establishment, Naka-machi, Naka-gun, Ibaraki-ken 311-0193, Japan

Abstract

In ELMy H-mode plasmas of Japan Atomic Energy Research Institute Tokamak-60 Upgrade, extension of a high confinement regime toward high density and high radiation-loss-power fraction has been investigated by Ar injection. With injecting Ar and putting the outer strike point on the top of divertor dome, confinement improvement, electron density, and radiation-loss-power fraction reached the ITER relevant regime; the thermal energy confinement time was as high as that the International Tokamak Experimental Reactor ELMy H-mode scaling IPB98$(y,2)$, the electron density is ~80% of the Greenwald density, and the radiation-loss-power fraction is ~0.8. Although electron density profile is slightly peaked with Ar injection, the confinement improvement is mainly attributed to the improvement of ion transport. Moreover, the maximum divertor heat load due to ELMs has been reduced by a factor of 3–5 with keeping high confinement. ELM activity can be controlled by injecting Ar and changing the strike point position.

PACS: 52.40.Hf
Keywords: Ar injection; Heat load reduction; ELM; High confinement; High density; JT-60U

1. Introduction

Control of divertor heat load in high performance plasmas is one of crucial issues for fusion devices. ITER requires high confinement ELMy H-mode plasmas with $HH_{98(y,2)} = 1$, radiation-loss-power fraction (P_{rad}/P_{heat}) of ~0.7, and high plasma purity (n_i/n_e) of ~80% at the density of ~0.85 n_{GW}, where $HH_{98(y,2)}$ is the improvement of thermal confinement energy time compared with IPB98$(y,2)$ scaling [1], P_{rad} is radiation loss power, P_{heat} is net heating power, n_i is fuel ion density, n_e is electron density, and n_{GW} is the Greenwald density, respectively. Higher radiation loss power up to ~80% is also desired. It is known that the confinement is degraded at high density in some large tokamaks [2,3]. Another requirement is heat reduction in the divertor. There are two types of divertor heat load, and those are the steady-state heat load and the transient heat load, respectively. Especially, large ELMs may limit the lifetime of divertor tiles. Therefore, the method is necessary for the reduction of ELM heat load with simultaneous achievement of high density, high radiation loss power, and high confinement.

Impurity injection is one candidate to reduce divertor heat load by radiation enhancement with high confinement at high density [4–10]. In Japan Atomic Energy Research Institute Tokamak-60 Upgrade (JT-60U), when the density is increased by deuterium gas puff only, the high confinement regime of $HH_{98(y,2)} \sim 1$ is limited in the region of $P_{rad}/P_{heat} < 0.4$ at $\bar{n}_e < 0.45\ n_{GW}$. Large ELMs are observed in this case. As shown in the 13th PSI conference, argon injection could extend the high performance plasmas of $HH_{98(y,2)} \sim 1$ to the range of $P_{rad}/P_{heat} \sim 0.8$ at $\bar{n}_e \sim 0.66\ n_{GW}$ [4]. However, the electron density was lower than ITER requirement, and

* Corresponding author. Tel.: +81-29 270 7349/7532; fax: +81-29 270 7419.
E-mail address: higashij@naka.jaeri.go.jp (S. Higashijima).

0022-3115/03/$ - see front matter
PII: S0022-3115(02)01502-7

large ELMs harmful to the divertor plates could not be disappeared. In order to extend the density regime with high confinement and high radiation-loss-power fraction, we made two attempts. The first is 'dome-top' configuration that the outer strike point is located on the dome top, and the second is 'high triangularity' configuration.

In this paper, heat load reduction, radiation enhancement, change of ELM activity are discussed in Ar injected plasmas. In Section 2, the JT-60U tokamak and diagnostics are presented. In Section 3 we present the plasma configurations (standard, dome-top and high triangularity configurations) and experimental results: confinement improvement and radiation enhancement, radial profiles of temperature and density, pedestal characteristics and ELM heat load. In Section 4, we discuss rapid change of the ELM frequency by injecting Ar and changing the position of the strike point. And an application of the dome-top configuration for the fusion devices is discussed. Finally, in Section 5, we summarize results and suggestions.

2. Experimental setup

JT-60U is a tokamak device with a major radius of 3.4 m and a minor radius of 1.1 m/1.4 m. Major modification of w-shaped divertor was carried out in 1998 [11], and the divertor consists of inner and outer baffle plates, divertor target tiles, a private dome and two toroidally continuous pumping slots in Fig. 1. In the w-shaped divertor, particles are exhausted through the two pumping slots near the inner and the outer legs in the private flux region. Particles from the inner leg side are conducted under the divertor dome and outer baffles and led to three cryo-pumps with particles from the outer leg side. Outer pumping enables to exhaust particles through the outer divertor for high triangularity plasma configuration in which the inner strike point is far from the inner pumping slot. Deuterium gas is puffed from the top of the main plasma, and argon puffing is carried out from the outer baffles to main plasma.

Key parameters in this experiment are as follows; electron density and electron temperature, ion temperature, impurity content, radiation loss power, and divertor heat load. Electron density is measured with a far-infrared laser interferometer (FIR) system and Thomson scattering systems. FIR system is used for the feedback-control of the main plasma density in this experiment. Thomson scattering system has two species of lasers, and they are Ruby laser and YAG laser. Ruby Thomson scattering system has 80 spatial channels in the upper half of the main plasma, and the time resolution is 4 s. YAG Thomson scattering has 14 spatial channels in the lower half of main plasma, and its time resolution is 20 ms. Electron temperature profile is also measured with these Thomson scattering systems. Ion temperature profile is estimated from charge exchange recombination spectroscopy (CXRS). The CXRS usually measures a recombination emission of C VI ($n = 8$–7, 529.2 nm). Time resolution is 16 ms, and spatial resolution is ~5 cm in the core region and ~1 cm in the pedestal region, respectively. Carbon density (C^{6+}) profile is also determined by CXRS system. Z_{eff} values are determined by visible Bremsstrahlung emission (wavelength ~523.0 nm), and this system has a 14-channel optical fiber array

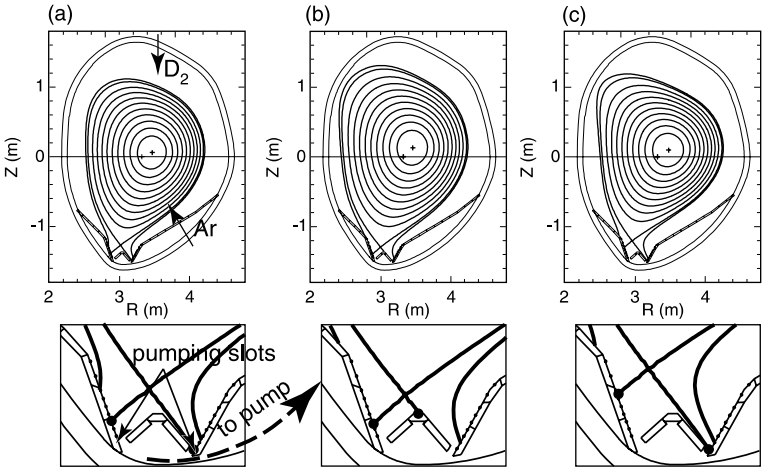

Fig. 1. Three configurations in this experiment: (a) standard; the triangularity $\delta = 0.36$, and the safety factor at 95% flux surface $q_{95} = 3.4$, (b) dome-top; $\delta = 0.37$ and $q_{95} = 4.1$, (c) high-d; $\delta = 0.50$ and $q_{95} = 3.7$. The lower figures show the divertor region. Deuterium puff: from the top of the main plasma, Ar puff: from the outer baffle. Particles are pumped out from two pumping slots to cryo-pumps.

and temporal resolution of 10 ms. Behaviors of intrinsic impurities and injected Ar are monitored on a VUV spectrometer. In order to measure radiation loss power in the main plasma, two bolometer arrays are installed, and the arrays totally have 31 viewing chords. A bolometer array viewing the upper half of the main plasma is used for feedback control of edge radiation [4,12]. IRTV camera [13] measures the divertor surface temperature and estimates heat flux of an ELM. Time resolution of this camera is 250 μs which is enough to measure ELM heat load, and its measuring time is 1.2 s.

3. Experiments

3.1. Plasma configurations

Ar injection experiments have been performed in ELMy H-mode plasmas with three plasma configurations shown in Fig. 1. Those are (a) standard configuration with the triangularity, δ, of $\sim$0.35 that the both strike points are located on the divertor, (b) dome-top configuration with $\delta \sim 0.35$ that the outer strike point is located on the dome top and (c) high triangularity configuration with δ of $\sim$0.5 that the both strike points are located on the divertor plate. The common plasma parameters are the plasma current of 1.2 MA, the toroidal magnetic filed of 2.5 T, the safety factor at 95% flux surface of 3.4–4.1 that is slightly larger than ITER requirement, and the injection power of NBI of 15–17 MW. Weak Ar injection and moderate deuterium puffing are applied to the main plasma. The Greenwald density limit was 5.4, 5.0 and 5.1×10^{19} m^{-3} for the standard, dome-top and high triangularity configurations, respectively.

In the dome-top configuration, an efficient fueling of deuterium and argon is expected due to particle recycling near the x-point in order to access to the higher density region. For the dome-top and standard configuration at $\bar{n}_e \sim 0.4\ n_{GW}$, the same amount of Ar gas of 0.11 Pa m^3/s was injected. The Z_{eff} value and Ar XV line emission were larger in the dome-top configuration than in the standard configuration. In the case of a constant hydrogen gas puff of 10 Pa m^3/s, achieved $\bar{n}_e$ was also higher in the dome-top configuration than in the standard configuration, and we confirmed the efficient fueling. Here, in order to understand this phenomenon, we tried to change Ar shielding. A constant hydrogen puff of 10 Pa m^3/s and a constant Ar puff of 0.11 Pa m^3/s were carried out simultaneously. Hydrogen puff, however, was too strong to separate the penetration and the pumping of Ar because of the perfect shielding of injected Ar by so-called 'puff and pump' effect [14]. There are other remarkable characteristics in the dome-top configuration. The dome-top configuration has a possibility to control an ELM heat load to the divertor, and the results are discussed in Section 3.5. Therefore, we investigated the dome-top configuration in detail.

In the high triangularity configuration without Ar injection, the confinement has been improved due to a high critical edge pressure gradient [15] and large ELMs, so-called type-I ELMs, which are considered harmful to the divertor plates in ITER, disappeared. Here, we injected Ar to the high triangularity configuration with high potential for the higher performance.

3.2. Confinement improvement and radiation enhancement

Fig. 2(a) shows the change of $HH_{98(y,2)}$ against the $\bar{n}_e/n_{GW}$. In the standard configuration without Ar injection, $HH_{98(y,2)}$ decreased from 0.9 to 0.6 as the $\bar{n}_e/n_{GW}$ increased from 0.45 to 0.66. On the other hand, the $HH_{98(y,2)}$ was kept high in the case of Ar injection. In the standard configuration, the $HH_{98(y,2)}$ remained $\sim$1 by $\bar{n}_e \sim 0.66\ n_{GW}$, but it rapidly decreased around 0.7 n_{GW} and the high confinement regime could not extend to

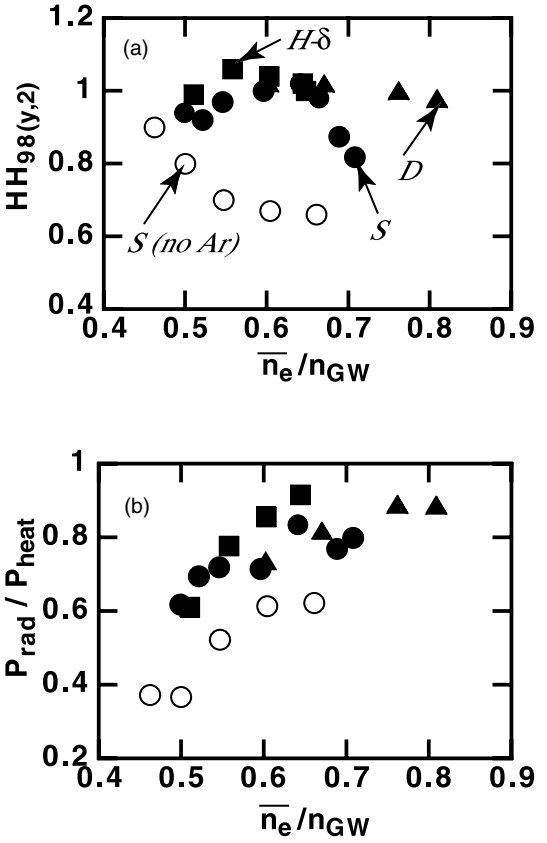

Fig. 2. (a) $HH_{98(y,2)}$ and (b) radiation loss power fraction as a function of electron density normalized by n_{GW}. Open circles: standard without Ar injection, Closed circles, triangles and squares: standard, dome-top, high-δ with Ar injection, respectively.

high density region. The $HH_{98(y,2)}$ in the dome-top case remained ~1 by the density range of 0.8 n_{GW}. The $HH_{98(y,2)}$ factor was higher in the high triangularity case than in the standard case. However, the $\bar{n}_e$ range could not extend over 0.66 n_{GW} so far. Further optimization is needed for the n_e extension in this case. For the confinement, the improvement by ~50% could be achieved at 0.66 n_{GW} compared with the case of no Ar injection. Here, the dominant intrinsic impurity in JT-60U is carbon, and the carbon density was not affected by Ar injection. The Ar concentration, n_{Ar}/n_e, was ~0.8% in these Ar injection cases. The fuel purity, the ratio of deuterium ion density to the n_e, n_D/n_e, was decreased from ~80% to ~60% at 0.66 n_{GW}. As a result, the value of $n_D \times \tau_E^{th}$, where τ_E^{th} is the confinement time of thermal energy, was increased by ~20% by Ar injection, and furthermore the fusion product, $n_i(0)\tau_E T_i(0)$, where $n_i(0)$ and $T_i(0)$ are the deuterium ion density and temperature at the center, was increased from 1.5 to 4.4×10^{19} m^{-3} s keV because of a significant confinement improvement.

Fig. 2(b) shows radiation-loss-power fraction as a function of the $\bar{n}_e/\bar{n}_{GW}$. The radiation-loss-power fraction increased with the density. With Ar injection, the radiation-loss-power fraction could achieve ~80% in the n_e range above 0.66 n_{GW} in all the cases. The ratio of the radiation loss power from the main plasma to total radiation loss power was ~60% and ~20% with and without Ar injection, respectively.

3.3. Radial profile of temperature and density and pedestal characteristics

Fig. 3 shows the profiles of the ion temperature, electron temperature and electron density in the main plasma without Ar injection ($HH_{98(y,2)} \sim 0.7$) and with Ar injection ($HH_{98(y,2)} \sim 1$) at the density of ~0.66 n_{GW}. Ar injected plasmas have higher ion temperature and electron temperature even with high radiation loss power. The ion temperature increased for the whole minor radius with Ar injection. The increase percentage of the electron temperature was smaller than that of the ion temperature. It suggests that the confinement improvement with Ar injection is attributed to the improvement of ion transport. For the electron density, the profile was slightly peaked with Ar injection, but strongly peaked profiles observed in 'RI-mode' plasmas [6] could not be obtained. Argon and carbon density profiles were flat in Ar injected plasmas, and impurity accumulation was not observed although Ar injected plasmas has the higher confinement.

Without Ar injection, the pedestal ion temperature decreased with the density in the standard, the dome-top and the high triangularity cases. On the other hand, high ion temperature remained in Ar injected plasmas [6]. Pedestal stored energy did not depend on Ar injection,

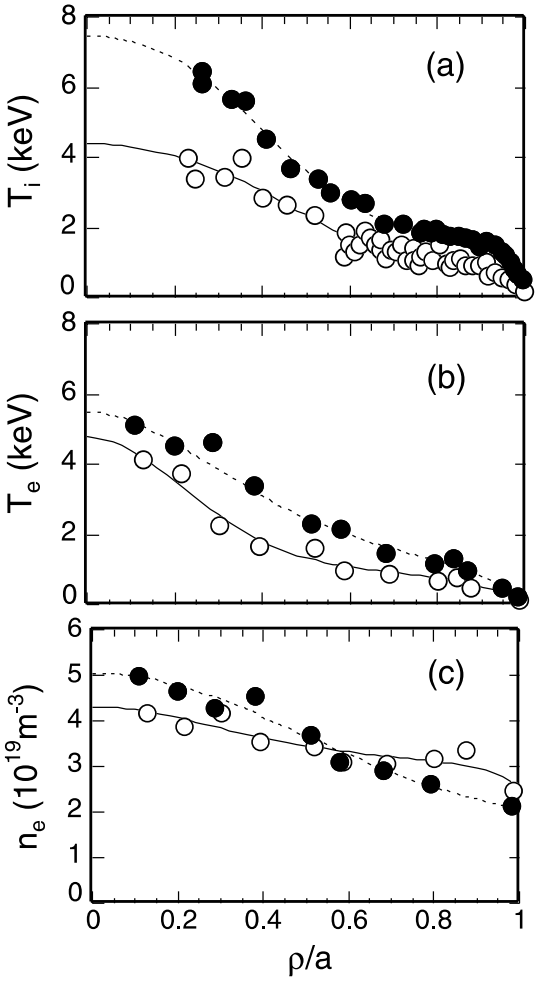

Fig. 3. (a) Ion temperature profiles, (b) electron temperature profiles and (c) electron density profiles in the standard configuration at the density of ~0.66 n_{GW}. Open circles; without Ar injection, closed circles; with Ar injection.

the density and the configurations, and it was kept constant in all the cases. An increase of core stored energy is dominant for the confinement improvement.

In Ar seeded plasmas, the shape of ion temperature profiles, $\log T_i$, inside the pedestal does not change with the electron density, and they have so-called 'stiff profile'. Therefore, the high pedestal ion temperature leads to high confinement. Although the weak density peaking is obtained with Ar injection, this contribution is small, and the main mechanism of the improvement confinement is different from that of RI-mode.

3.4. Reduction of ELM heat load by injecting Ar

Time history of heat flux near the inner strike point is shown in Fig. 4. These data were obtained in ELMy

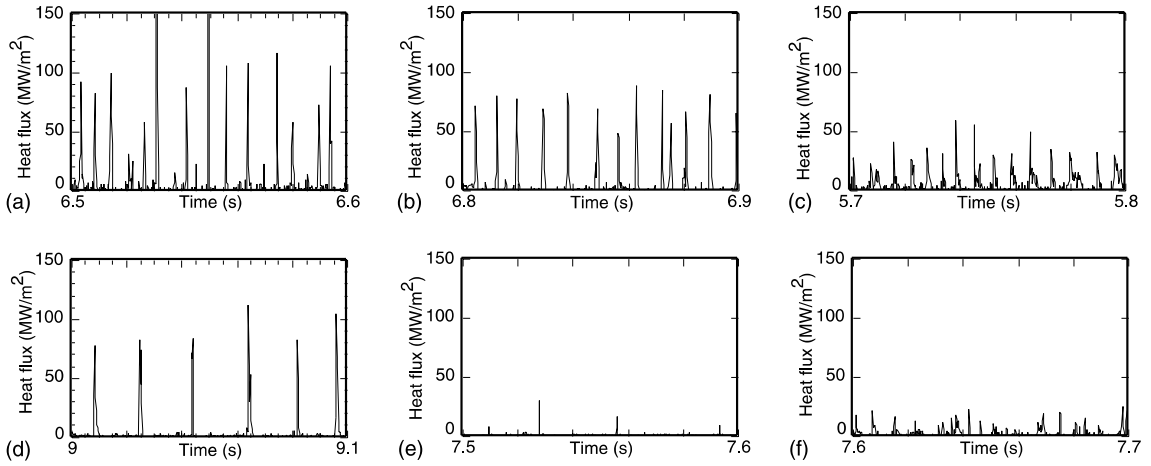

Fig. 4. Heat flux due to ELMs at the inner strike point at $HH_{98(y,2)} \sim 0.95$. Left figures (a) and (d); standard, middle figures (b) and (e); dome-top, and right figures (c) and (f); high-δ. Upper figures (a)–(c): without Ar injection, lower figures (d)–(f): with Ar injection. The electron density is (a) 0.49 n_{GW}, (b) 0.52 n_{GW}, (c) 0.45 n_{GW}, (d) 0.64 n_{GW}, (e) 0.70 n_{GW}, (f) 0.60 n_{GW}, respectively.

H-mode plasmas with the high confinement of $HH_{98(y,2)}$ factor around 0.95. Heat flux due to ELMs was high near the inner strike point for all the cases, although the steady-state heat flux measured with a slow-sampled IRTV camera was observed at the outer strike point. Fig. 4 (a) and (d), (b) and (e), and (c) and (f) are the standard, the dome-top, the high-δ cases, respectively. And the upper three figures of Fig. 4 (a)–(c) show data without Ar injection, and the lower figures of Fig. 4(d)–(f) show data with Ar injection. Even without Ar injection, by taking the dome configuration, the amplitude of ELM heat flux was slightly reduced. And, by taking the high-δ configuration, the ELM amplitude was also reduced, and it might be explained by access to the second stability for ideal ballooning modes.

Then, with Ar injection, we could change the ELM activity drastically. In the standard case, the ELM frequency decreased, while the amplitude did not decrease. In the dome-top case, the frequency and the amplitude of ELMs were reduced by Ar injection. In the high-δ case, the ELM amplitude decreased, but the ELM frequency did not decrease.

Fig. 5(a) shows the time-averaged ELM deposited energy (integration over 0.1 s) to the divertor as a function of the n_{GW} without Ar injection and with Ar injection when the $HH_{98(y,2)}$ factor was between 0.9 and 1. The ELM heat load with high confinement could be reduced by Ar injection by a factor of 3–5.

Here, the mechanism of heat load reduction with Ar injection are summarized from the stand point of the frequency, the maximum heat flux, the decay time, and the width of ELMs. Fig. 5(b) shows ELM frequency as a function of the Greenwald density fraction. In the standard case, the frequency rapidly decreased just after Ar injection and then it gradually decreased with the density. This rapid change of ELM frequency is discussed in Section 4. In the dome-top case, the frequency gradually decreased with the density. On the other hand,

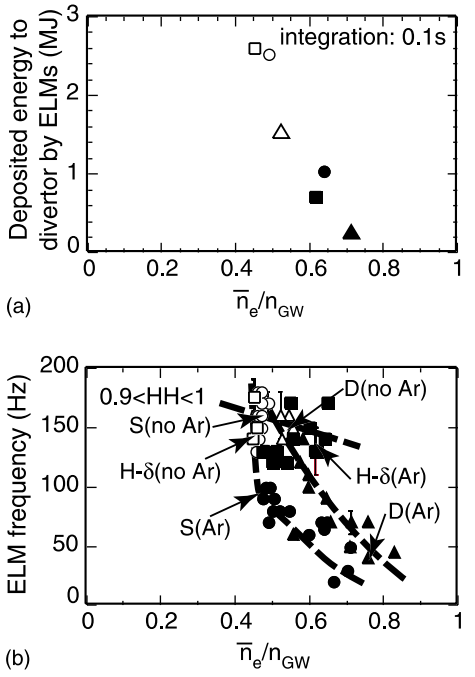

Fig. 5. (a) Time-integrated deposited energy to divertor due to ELMs, (b) ELM frequency as a function of electron density normalized by n_{GW} with high confinement of $HH_{98(y,2)} = 0.9$–1.0. Open symbols; without Ar injection and closed symbols; with Ar injection. Circles; standard, triangles; dome-top, squares; high-δ, respectively.

the frequency was almost constant in the high-δ case. Next, the maximum heat flux, q_{max}, due to an ELM is estimated for the case without Ar injection and for the case with Ar injection. In the standard case, the q_{max} was 100–120 MW/m^2 without Ar injection and ~100 MW/m^2 with Ar injection, and the value did not change by Ar injection. In the dome-top case, by Ar injection, the q_{max} decreased from ~80 MW/m^2 to ~20 MW/m^2. In the high-δ case, the q_{max} of 30–60 MW/m^2 decreased to 20–30 MW/m^2. Finally, we discuss the decay time of q_{max}, Δt, that is defined as the time that the q_{max} decreases to the background heat flux. In all the cases, the Δt did not change so much by Ar injection. The values of the Δt without and with Ar injection are as follows; ~0.9 to ~1.0 ms in the standard case, ~1.3 to ~1.3 ms in the dome-top case, and ~1.9 to ~1.9 ms in the high-δ case, respectively. The interesting point is that the Δt is longer in the high-δ case than in the standard and the dome-top cases. In the high-δ case, high deposited power can be explained by this longer Δt although the q_{max} is small. And this longer Δt in the high-δ case might be explained by the difference of the ELM type (type-I in the standard case and type-II in the high-δ case). Here, from the above results, the mechanism of the heat load reduction by Ar injection is as follows. In the standard case, the heat load reduction is attributed to the reduction of the frequency. In the dome-top case, the heat load reduction is caused by the reduction of both the frequency and the q_{max}. In the high-δ case, the reduction of q_{max} is key.

Next, the profiles of ELM heat flux are discussed in the inboard divertor. Here, the width of ELM heat flux, λ, in the divertor is defined as Q over q_{max}, where Q is integrated heat flux over the inboard divertor. The width is converted to the length in the outer midplane because of three different configurations. Fig. 6 shows the relation between λ and Q. In the standard and the dome-top cases, the width of ELM heat flux generally does not change. On the other hand, in the high-δ cases, the width decreases by Ar injection. Here, these results are discussed from the standpoint of the pedestal parameters in the ELMy H-mode plasmas with the high confinement of $HH_{98(y,2)} \sim 0.95$. The pedestal ion temperature was almost constant in all the cases. The pedestal ion density was also constant although the $\bar{n}_e$ increased because of high $\bar{n}_e/n_{GW}$ in Ar injected case. Therefore, Ar injection did not change the ion pedestal pressure and the ion collisionality. For the electron, the pedestal electron density was higher with Ar injection than without Ar injection because of high $\bar{n}_e/n_{GW}$ in Ar injected case. The error of the electron temperature was large in these discharges, and electron pedestal pressure was not clear. Therefore, the estimation of the electron pedestal parameters is our future work. Furthermore, the parallel transport should be considered. Anyway, further study is required for understanding the Ar effect on the width profiles.

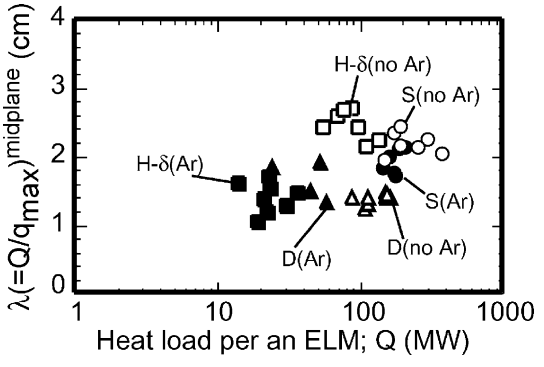

Fig. 6. Width, λ, of ELM heat flux as a function of heat load per an ELM, Q, at $HH_{98(y,2)} \sim 0.95$. Open symbols; without Ar injection and closed symbols; with Ar injection. Circles; standard, triangles; dome-top, squares; high-δ, respectively.

3.5. Reduction of ELM heat load by changing the divertor geometry

In Ar injected ELMy H-mode plasmas with $I_p = 1.2$ MA, $B_t = 2.5$ T and $HH_{98(y,2)} \sim 1$, the outer strike point position was moved from the dome-top to the dome-side in Fig. 7. The dome-top configuration was kept by 9.4 s, and then the configuration was changed and fixed at 9.9 s. A constant Ar puff was applied until 10.0 s, and deuterium was not puffed during this period. Electron density, radiation loss power, Ar XV line emission, NB heating power, stored energy were almost constant during this phase. However, after changing the strike point position, the ELM activity shown in D_α line intensity changed rapidly to type-I ELMs when the radial (R-) position of the outer strike point changed slightly.

Then, key pedestal parameters for ELM activities such as triangularity δ, safety factor at 95% of minor radius q_{95}, ion collisionality ν^*_{i95}, ion temperature gradient at the shoulder of the pedestal $\nabla(T_i)^{PED}$, and pedestal stored energy W^{PED} were almost the same. The values of these parameters are as follows; $\delta = 0.36$, $q_{95} = 4.1$, $\nu^*_{i95} = 0.49$, $\nabla(T_i)^{PED} = 0.11$ keV/cm, $W^{PED} = 0.58$ MJ at 9.4 s, and $\delta = 0.36$, $q_{95} = 4.0$, $\nu^*_{i95} = 0.40$, $\nabla(T_i)^{PED} = 0.10$ keV/cm, $W^{PED} = 0.59$ MJ at 9.9 s, respectively. Therefore, this cannot be explained as MHD phenomena.

Although the mechanism of this change of ELM activity is unclear at present, we speculate that the plasma near the x-point changes locally by changing the strike point position and consequently the edge plasma might be changed. For further understanding this phenomenon, the local measurements near the x-point are essential. Another conceivable effect on this phenomenon is wall condition. It is observed that the ELM activity in good wall condition was different from that in

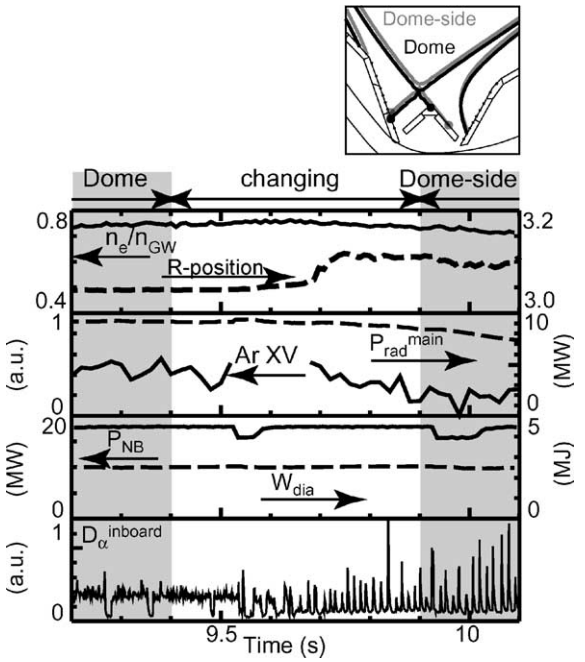

Fig. 7. Time history of electron density normalized by n_{GW}, radial position of the outer strike point, Ar XV line emission, radiation power from the main plasma, NB heating power, stored energy, and D_α line emission in the inboard divertor. Ar XV line emission could not be measured from ~9.5 to 9.7 s because of the noise. The outer strike point position was moved from the dome-top (9.4 s) to the dome-side (9.9 s).

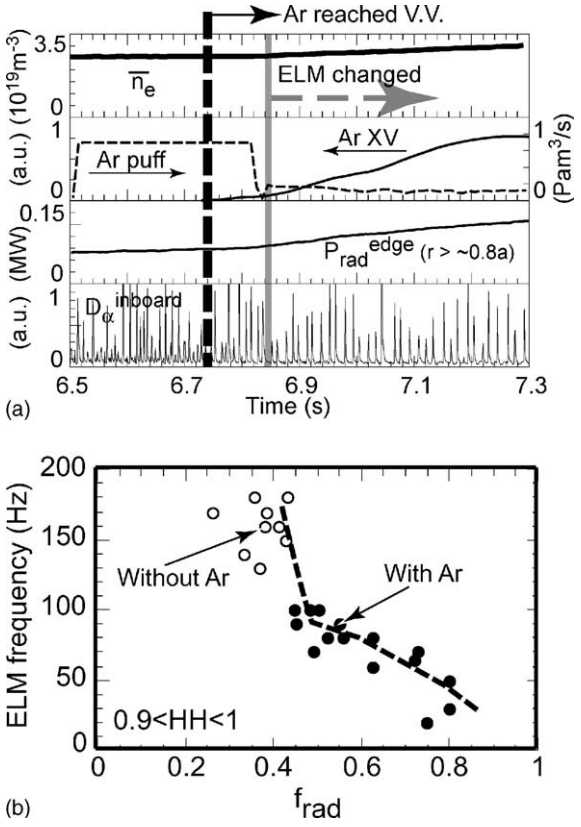

Fig. 8. (a) Time history of electron density, Ar XV line emission, preprogrammed Ar puffing rate, radiation power from the edge plasma, and D_α line emission in the standard case, (b) ELM frequency as a function of radiation-loss-power fraction in this case.

bad wall condition [16]. Before executing this discharge, the ELMy H-mode plasmas with the dome-top configuration had been repeated for many times, and a prominent increase of D_α line emission, which is seen in the bad wall condition, was not observed at the top of the dome. In addition, high performance plasma with $HH_{98(y,2)} \sim 1$ cannot be obtained in the bad wall condition of JT-60U. Therefore, this phenomenon can be separated from the wall condition although the ELM activity depends on the wall condition. And this change of the ELM activity was also observed in ELMy H-mode plasmas without Ar injection, and this phenomenon is not related to Ar injection.

So, we emphasize that the ELM activity can be changed by changing the strike point position although the mechanism is still open question.

4. Discussion

In the standard configuration, the rapid reduction of the ELM frequency was observed just after Ar injection. Someone might guess that the reduction can be explained by radiation enhancement, but the guess is contradicted here. Fig. 8(a) shows the time behavior of the density, Ar XV line emission, preprogrammed Ar puffing rate, radiation loss power from the edge region, and D_α line emission in the inboard divertor in the standard case. Ar puffing was carried out from 6.5 s, and Ar reached the vacuum vessel at ~6.74 s because the location of Ar puffing is far from the vacuum vessel and it takes ~0.25 s to reach the vacuum vessel. In this period, deuterium gas puffing was not applied. Just after Ar reached the vacuum vessel, the ELM frequency rapidly decreased to ~1/2 of the frequency shown in Fig. 8(b). However, the increases in the density, radiation loss power from both the edge and the main, and Ar XV line emission were small at that time. Therefore, the decrease in the ELM frequency cannot be explained by an increasing in reheating time due to a decrease in the edge heating power by the edge radiation.

The application of the dome-top configuration is discussed for the fusion devices. As we described the above, the dome-top configuration has some advantages such as the achievement of the high confinement with Ar injection at the high density, efficient fueling of particle

from the x-point and reduction of the ELM activity. Transient heat flux due to ELMs does not come to the dome-top, but the dome receives 2–4 MW/m^2 of the steady-state heat flux in ELMy H-mode plasmas with ~17 MW of NB heating. So, the application of the dome-top configuration is difficult in the present condition. For us, the dome-top configuration is positioned as one of the methods to extend the operational region by efficient fueling and control of the ELM activity. If we understand the mechanisms of the dome-top configuration, we might be able to reach something other than the dome-top configuration.

5. Summary

With Ar injection and the dome-top configuration, high confinement regime with high radiation loss power has been extended to high density region in ELMy H-mode plasmas of JT-60U. The confinement improvement, electron density, and radiation-loss-power fraction reached ITER relevant regime; $HH_{98(y,2)}$ is ~1, the electron density is ~0.8 n_{GW}, and radiation-loss-power fraction is ~0.8, although q_{95} is ~4 that is slightly larger than ITER requirement. With Ar injection, electron density profile is slightly peaked, but the confinement improvement is attributed to the improvement of ion transport.

The maximum heat flux has been reduced by a factor of 3–5 with keeping high confinement with Ar injection. The heat load reduction with Ar injection is attributed to the reduction of the frequency in the standard case, the reduction of both the frequency and the q_{max} in the dome-top case, and the reduction of the q_{max} in the high-δ case, respectively. For the change of the width of ELM heat flux with Ar, the width does not change in the standard and the dome-top cases, and the width decreases in the high-δ cases. Moreover, the ELM activity can be reduced by changing the strike point position. However, this reduction of the ELM activity cannot be explained as MHD phenomena. In order to establish the ELM control, we emphasize that an investigation of effect of impurity and divertor geometry is necessary.

Acknowledgements

The authors are grateful to the JT-60 team for excellent cooperation. The authors would like to thank Drs A. Kitsunezaki, H. Ninomiya and M. Kikuchi for continuous support. The authors would like to thank Drs T. Takizuka and M. Shimada for useful and helpful discussion.

References

[1] ITER EDA documentation series no. 18, ITER-FEAT outline design report, International Atomic Energy Agency, Vienna, 2001.
[2] N. Asakura et al., Plasma Phys. Control. Fusion 39 (1997) 1295.
[3] JET team, Nucl. Fusion 39 (1999) 1687.
[4] S. Sakurai et al., J. Nucl. Mater. 290–293 (2001) 1002.
[5] H. Kubo et al., Nucl. Fusion 41 (2001) 227.
[6] H. Kubo et al., Phys. Plasmas 9 (2002) 2127.
[7] U. Samm et al., Plasma Phys. Control. Fusion 35 (1993) B167.
[8] O. Gruber et al., Phys. Rev. Lett. 74 (1995) 4217.
[9] M.R. Wade et al., J. Nucl. Mater. 290–293 (2001) 44.
[10] J. Ongena et al., Phys. Plasmas 8 (2001) 2188.
[11] N. Hosogane et al., in Plasma Phys. Control. Nucl. Fusion Research 1996, Proceedings of the 16th International Conference, Montreal, 1996, vol. 3, IAEA Vienna, 1996, p. 555.
[12] S. Konoshima et al., these Proceedings.
[13] K. Itami et al., J. Nucl. Mater. 196–198 (1992) 755.
[14] N. Hosogane et al., Plasma Phys. Control. Nucl. Fusion Research 1998, Proceedings of the 17th International Conference, Yokohama, 1998, vol. 3, IAEA Vienna, 1999, p. 903.
[15] Y. Kamada et al., Plasma Phys. Control. Fusion 44 (2002) A279.
[16] A. Chankin et al., these Proceedings.